ARTICLE   OPEN

Check for updates

Mediator-assisted synthesis of WS$_2$ with ultrahigh-optoelectronic performance at multi-wafer scale

Yu-Siang Chen[1], Sheng-Kuei Chiu [2], De-Liang Tsai[3], Chong-Yo Liu[4], Hsiang-An Ting[5], Yu-Chi Yao[4], Hyungbin Son[6], Golam Haider [7], Martin Kalbáč[7], Chu-Chi Ting[3], Yang-Fang Chen [4], Mario Hofmann [4] and Ya-Ping Hsieh [1]✉

The integration of 2D materials into future applications relies on advances in their quality and production. We here report a synthesis method that achieves ultrahigh optoelectronic performance at unprecedented fabrication scales. A mediator-assisted chemical vapor deposition process yields tungsten-disulfide (WS$_2$) with near-unity photoluminescence quantum yield, superior photosensitivity and improved environmental stability. This enhancement is due to the decrease in the density of lattice defects and charge traps brought about by the self-regulating nature of the growth process. This robustness in the presence of precursor variability enables the high-throughput growth in atomically confined stacks and achieves uniform synthesis of single-layer WS$_2$ on dozens of closely packed wafers. Our approach enhances the scientific and commercial potential of 2D materials as demonstrated in producing large-scale arrays of record-breaking optoelectronic devices.

INTRODUCTION

2D materials are atomically thin structures that have been heralded as enabling materials for optoelectronics, energy devices, and sensors[1]. To support such research directions and realize future applications, however, the quality of 2D materials has to be improved. One of the most pressing issues is the enhancement of 2D materials' uniformity both at the nanoscale and the macroscale. Atomic discontinuities, such as vacancies and lattice defects lower the carrier mobility, enhance nonradiative recombination, and deteriorate the chemical stability of 2D materials[2]. Macroscopic variations in coverage and thickness, on the other hand, introduce tilt boundaries, modify the band structure, and lower the compatibility with large-scale semiconductor fabrication techniques[3]. The challenges posed by uniformity are exemplified in Tungsten disulfide (WS$_2$) a transition metal dichalchogenide that is promising as material in electronics, valleytronics, and optics[1,4]. Nonuniformity in WS$_2$ reduces the experimentally obtained carrier mobility to less than 10% of theoretical predictions[5,6] and the quantum yield to a fraction of its extrinsically controlled value[7]. Furthermore, non-uniform WS$_2$ suffers from environmental degradation if exposed to ambient conditions[8]. Therefore, an approach is needed that can enhance the uniformity of 2D materials at all relevant length scales. This issue is even more pressing as mechanical exfoliation from bulk TMDCs does not produce comparably high-quality material as in the case of graphene exfoliation from graphite[9,10].

We here introduce a novel synthesis process that can produce WS$_2$ with superior uniformity at both the nanoscale and the macroscale. Mediator-assisted WS$_2$ growth was shown to enhance the robustness of WS$_2$ growth by stabilizing the reaction rate in the presence of supply variability. This approach yields WS$_2$ with defect concentrations below the levels of material available by exfoliation or CVD synthesis. The absence of charge traps was

shown to increase the quantum yield of intrinsic WS$_2$ to near-unity, which is promising for future optoelectronics. Moreover, the large size of single-crystalline grain reduces the concentration of dangling bonds which results in excellent environmental stability. The mediator-stabilized supply of precursor furthermore enables high and uniform growth rates under fluid dynamical confinement and allows us to increase the production throughput by more than 10x compared to traditional CVD growth. This advance was illustrated by producing uniform single-layer WS$_2$ on dozens of tightly packed wafers with an equivalent size corresponding to an 8"-wafer using a simple, laboratory-scale furnace. The exciting potential of producing 2D materials with improved uniformity, quality, and scale of the material was illustrated by producing optoelectronic devices with superior performance.

RESULT AND DISCUSSION

Mediator-assisted growth process

TMDC growth by chemical vapor deposition faces additional challenges compared to graphene CVD which reliably produces continuous and uniform monolayer materials. One central issue is the supply of metal and chalcogen precursor, which has been the leading cause of both atomic and macroscopic discontinuities. First, precursors have to be provided in a stoichiometric ratio to produce high-quality 2D materials[11]. Moreover, a time-invariant precursor supply needs to be realized to maintain a fixed edge termination of the growing 2D material as otherwise structural defects are being introduced[12]. Finally, a high-concentration and uniform precursor supply is required to support large growth rates and ensure connectivity between neighboring grains[13].

These new requirements for producing high-quality 2D TMDCs are challenging for standard CVD processes. There is little control over precursors' spatial and temporal distribution due to the

[1]Institute of Atomic and Molecular Sciences, Academia Sinica, Taipei 10617, Taiwan. [2]Department of Material Science and Engineering, Feng Chia University, Taichung 40724, Taiwan. [3]Graduate Institute of Opto-Mechatronics, Department of Mechanical Engineering, National Chung Cheng University, Chia-Yi 62102, Taiwan. [4]Department of Physics, National Taiwan University, Taipei 10617, Taiwan. [5]Department of Mechanical Engineering, National Chiao Tung University, Hsinchu 30010, Taiwan. [6]School of Integrative Engineering, Chung-Ang University, Seoul 06974, Republic of Korea. [7]J. Heyrovsky Institute of Physical Chemistry of the Czech Academy of Sciences, Dolejškova 2155/3, 182 23 Prague, Czech Republic. ✉email: yphsieh@gate.sinica.edu.tw
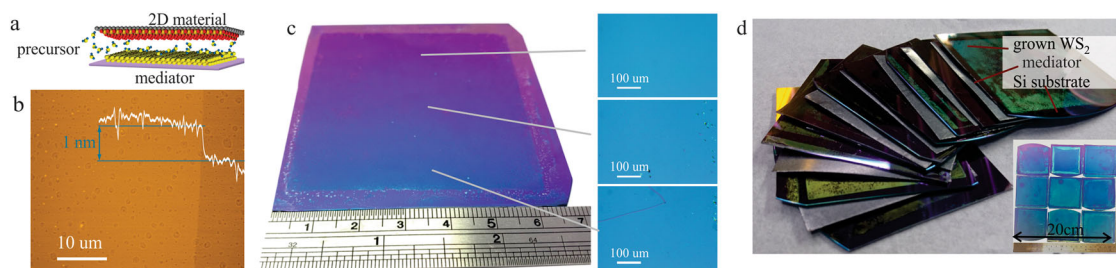
npj

Fig. 1 Scale of mediator-assisted CVD. a Schematic of mediator-assisted growth. **b** AFM image of mediator-assisted WS$_2$ growth result with overlaid cross-sectional height. **c** Photograph of large-scale WS$_2$ sample with optical micrographs taken at different locations indicating uniformity. **d** Photograph of WS$_2$ synthesized within a stack during a single growth batch, (inset) photograph of attained growth area from 3″ reactor growth.

combination of complex fluid transport and multistep gas- and surface-chemistry[14,15]. In chemistry, the stabilization of a reaction in the presence of precursor variability is achieved through a buffer solution, whose consumption does not affect the reaction but changes the concentration of intermediate species. In analogy to buffer solutions, we introduce a graphitic mediator that enhances and stabilizes the reactant supply by reaction with the precursor.

To realize this goal, we place a graphite film in direct contact with the substrate so that, during chemical vapor deposition, precursors interact with the mediator before being deposited on the substrate (Fig. 1a). Our process aims to enhance the WS$_2$ quality by modifying the kinetics of the growth process, which is in marked difference to previous routes that have focused on improving the epitaxy[16,17] and surface diffusion[18] of the growth substrate.

The success of this mediator-assisted growth approach can be seen when characterizing the WS$_2$ grown in this arrangement. First, atomic force microscopy (AFM) reveals highly uniform single-layer WS$_2$ (Fig. 1b) with no indication of discontinuities or bilayers. Optical microscopy demonstrates that the uniform contrast of single-layer WS$_2$ extends over large- scale (50 × 50 mm) on SiO$_2$/Si substrates (Fig. 1c) and is confirmed by statistical evaluation of spectroscopic data (Supplementary Fig. 4). Such a result is a significant advance over conventional CVD on any SiO$_2$/Si substrate, which can only produce WS$_2$ with significant spatial inhomogeneity due to the aforementioned precursor-supply challenges[19].

The unprecedented uniformity in mediator-assisted WS$_2$ growth can be increased further to the multiwafer scale (Fig. 1d). By employing a confined-stacking method similar to previously employed to the synthesis of graphene[20], the throughput of CVD production can be enhanced. The growth-scale in a research-scale 3″ growth reactor was extended to multiple wafers, which has an area equivalent to an 8″ wafer (Fig. 1d) (also See Supplementary Fig. 1). Future work will have to address the effect of outgassing from the graphite separators at the growth conditions, which introduces non-niform deposits. However, as our subsequent analysis demonstrates, these deposits are not affecting the optoelectronic performance of the produced material.

Growth mechanism

Our results represent a significant increase in WS$_2$ growth scale, grain size, and throughput compared to previous reports on TMDCs[21,22] and we will subsequently investigate the mechanism of the mediator-assisted growth. In analogy to chemical buffers, uniform growth in the presence of spatial variations of the precursor concentration requires a self-regulating process. To study if mediators can stabilize the precursor concentration, we modify the supply conditions within a single growth experiment. For this goal, we exploit the spatial change of fluid dynamical

conditions in confined growth processes. Previous work demonstrated the large difference of gaseous radical concentration in nanometer-scale gaps due to enhanced wall collisions in Knudsen diffusion[23].

When characterizing the growth rate of CVD-grown WS$_2$ at different locations of a sample that is brought in close contact with a solid cap (background of Fig. 2a), we observe that WS$_2$ growth in the center of the sample proceeds significantly slower than at the edges (Fig. 2a) as less sulfur reaches the center and can be converted into WS$_2$. Consequently, confined, conventional CVD's growth rate closely follows the sulfur supply's concentration profile (inset Fig. 2a).

Surprisingly, confined, mediator-assisted CVD growth demonstrates a constant growth rate independent of the pore position (Fig. 2a). This observation indicates that a mediator can stabilize the precursor concentration sufficiently so that a tenfold variation in the supply does not modify the growth rate appreciably. Such a remarkable and unprecedented stability of the WS$_2$ growth rate in the presence of large variations in the precursor supply explains the mediator's effect in improving the uniformity of 2D materials' growth.

Thermomechanical modeling was conducted to understand the mediator's observed effect on stabilizing precursor supply. For this purpose, the mass balance of tungsten oxide, carbon, hydrogen sulfide and tungsten sulfides was calculated by minimizing the free energy of their coupled reaction equations. Based on this method, the relation between the concentration of precursors and reaction products could be established in the presence of various mediator concentrations. (Details on the modeling can be found in the methods section). To characterize the sensitivity of growth conditions on sulfur precursor supply, we introduce a sensitivity factor ($\sigma = d[WS_2]/d[S]$) that represents the change in WS$_2$ concentration for small variations in sulfur concentration. We observe a large and positive sensitivity value in mediator-free growth that indicates a strong dependence of growth conditions on precursor supply in agreement with our results for conventional CVD growth (Fig. 2b). Upon addition of a mediator, a decrease of σ is observed and finally a complete independence of WS$_2$ concentration from sulfur supply can be achieved at sufficient mediator concentrations. This effect indicates that the mediator is being consumed during growth, which distinguishes our approach from catalytic CVD approaches. From these results, we would expect that the mediator will be consumed at a rate that is comparable to the growth rate of WS$_2$, indicating that a few graphene layers would be sufficient to mediate single-layer WS$_2$ growth. This prediction agrees with experimental findings as detailed in the Supplementary Note 1.

Modeling suggests that the experimentally observed decoupling of growth conditions from the supply concentration is realized by providing an alternative reaction pathway to tungsten oxide reduction. In common CVD, tungsten oxide precursor has to be reduced by hydrogen from the hydrogen sulfide precursor
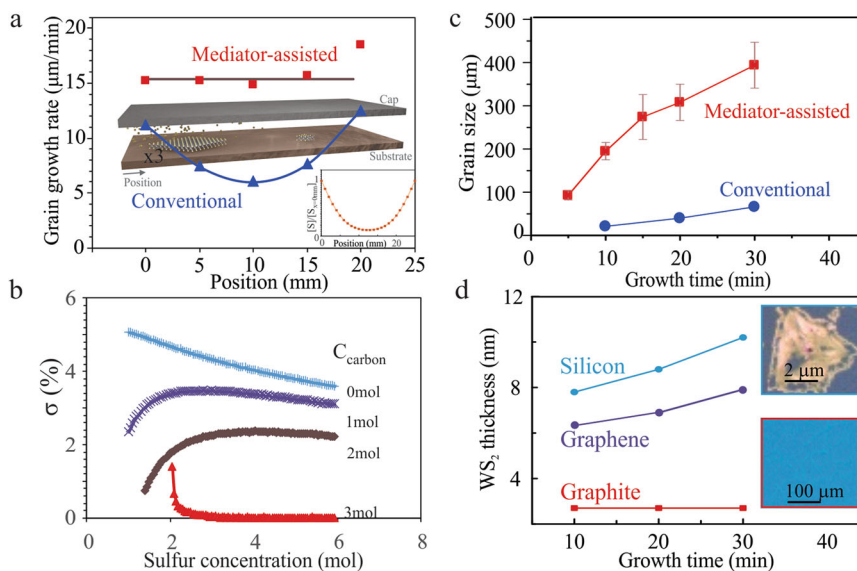
Fig. 2 Mediator-assisted growth process. a Characterization of grain growth rate within close confinement for mediator-assisted and mediator-free growth, (center inset) depiction of pore with indication of position origin, (bottom right inset) calculated concentration of sulfur in the same setup according to Chen et al[22]. **b** Thermochemical simulation of sensitivity factor σ at different concentrations of carbon-based mediator (more details in text). **c** Time-dependent WS_2 grain size for mediator-assisted and unassisted CVD. **d** Time evolution of WS_2 thickness for different types of mediators, (inset) optical micrographs of WS_2 grown without a mediator (top) and with a graphite mediator (bottom).

before being incorporated into WS_2. Our mediator provides a more efficient route for the tungsten precursor conversion, and sulfide precursor is only required for the growth step. Such simplification of multistep reactions is applicable to many current 2D materials' growth processes by CVD.

Another advantage of our mediator-assisted growth is an increased WS_2 growth rate. Time-dependent grain size measurements reveal that growth proceeds at least eight times faster than for mediator-free growth (Fig. 2c), highlighting the potential of mediator-assisted growth for high-efficiency 2D materials synthesis.

Finally, we observe that the growth process exhibits improved robustness when employing a mediator. The thickness of WS_2 grown without a mediator increases with growth duration, indicating the formation of multilayers through either layer-by-layer WS_2 growth[24] or co- deposition of $WO3$[25] (Fig. 2d). Mediator concentrations were varied by employing single-layer graphene or a graphite film (~200 μm), and it is shown that sufficiently high mediator concentrations can achieve a self-limiting WS_2 growth process (Fig. 2d)

Characterization of mediator-grown WS_2

Optical spectroscopy is a powerful tool for the characterization of WS_2 down to the atomic level. The variation in photoluminescence (PL) intensity can help to identify atomic vacancies, changes to stoichiometry, and occurring charge transfer processes[7]. Comparison of PL intensities for WS_2 from different sources (se Supplementary Note 2 for sample characterizations) demonstrates that mediator-growth produces a 10,000-fold enhancement over unmediated-CVD grown WS_2 and four times increase over exfoliated WS_2 (Fig. 3a).

To provide a quantitative comparison to previous results, we extract the quantum yield for these different WS_2 sources (Fig. 3b). Exfoliated WS_2 exhibits quantum yields of ~ 20%[26,] which agrees with previous work, while material grown by mediator-free CVD has a lower quantum yield. Mediator-grown WS_2 exhibits near-unity values, significantly outperforming conventional WS_2. We emphasize that this unprecedented high quantum yield was achieved without external charge transfer

to block trap states[27], indicating the potential of mediator-grown WS_2 for future optoelectronics[28.]

To elucidate the observed enhancement in emission for mediator-grown material, we conduct a detailed characterization of the PL spectra (inset Fig. 3a). A shift in the peak-positions of mediator-assisted WS_2 is attributed to strain, as confirmed by XPS analysis (Supplementary Fig. 5 and Supplementary Note 6). More importantly, the PL spectra of mediator-assisted WS_2 PL spectra show a high ratio of neutral excitons concentration to trions concentration compared to CVD grown and exfoliated material (Supplementary Fig. 6). Moreover, the suppression of defect-related PL transitions around 1.92 eV (with biexciton energy of ~65 meV)[29] indicates the enhanced quality of mediator-grown WS_2.

Statistical analysis of 10,000 PL spectra was conducted to quantify the impact of defects on WS_2's quantum yield. The PL peak width was correlated with the intensity for conventional CVD and mediator-assisted growth. A universal trend is observed in Fig. 3c for both sources that links a narrower width to higher emission efficiency. From this analysis it is apparent that trions and defect-bound excitons decrease the quantum yield and that the enhanced emission yield of mediator-grown WS_2 over previous results originates from the decreased impact of these transitions.

This enhancement in optoelectronic performance can be understood when analyzing PL maps of the WS_2 emission intensity. For conventionally grown WS_2, a complex spatial PL distribution is observed (inset Fig. 3c) that suggests large variability of crystal quality and the presence of reactive edges[7]. In contrast, mediator-grown material shows a uniform emission intensity across the film with only small intensity variations over large length scales (inset Fig. 3c) (more information See Supplementary Note 5). The minimization of reactive edges in mediator-grown material also enhances its environmental stability. Exposure to ambient environment was found to deteriorate exfoliated WS_2 within days whereas mediator-grown WS_2 remains stable over several months (Supplementary Fig. 8) which exceeds the stability of previous passivation approaches[30].

We further study the emission process by conducting power-dependent PL characterization (Fig. 3d). All grown materials exhibit a similar behavior at higher laser power where the
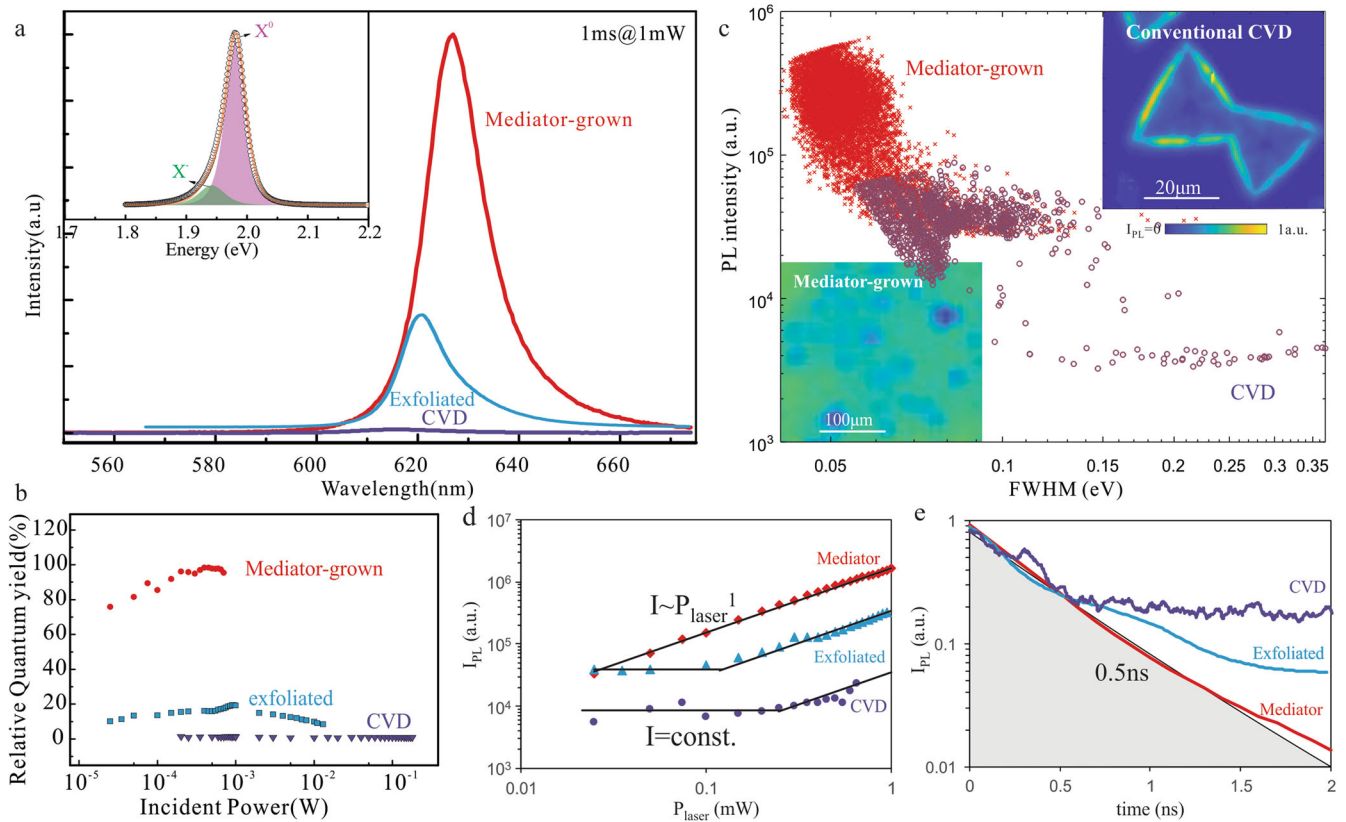
Fig. 3 **Optoelectronic properties of mediator-grown WS₂. a** Photoluminescence of WS₂ from different sources, (inset) PL spectrum of mediator-grown CVD grown WS₂ with deconvolution into neutral exciton (X0) and trion (X-) peak. **b** Quantum-yield measurements for WS₂ grown with/without a mediator and mechanically exfoliated WS₂. **c** Statistical analysis of PL peak width (Lorentzian FWHM) and PL intensity for different locations within samples produced by conventional and mediator-assisted CVD, (insets) spatial maps of emission intensity for different WS₂ sources. **d** PL intensity vs excitation power for different WS₂ sources with indication of constant and linearly varying components. **e** Time-resolved PL intensity for different WS₂ sources with indication of intrinsic response time.

emission intensity increases according to $I \sim P^k$, where I, P, and k represent the PL intensity, the laser power density, and the numerical power, respectively[31]. The numerical power is close to 1, which suggests the limited impact of non-radiative recombination through deep defect levels in all sources of WS₂[31]. However, for CVD growth and exfoliation, WS₂ exhibits a constant intensity at low excitation power. This behavior is indicative of the saturation of trap states associated with defects. We infer a significantly decreased concentration of trap states from the absence of such a constant-intensity tail in mediator-grown WS₂. This assessment is confirmed by time-resolved photoluminescence (TR-PL) measurements (Fig. 3e). The TR-PL spectra of all WS₂ sources show a short lifetime component of 0.5 ns representing the intrinsic radiative recombination rate at room temperature[32]. On the other hand, both exfoliated and mediator-free grown WS₂ show additional longer lifetime components that indicate defect induced exciton trapping[27]. The absence of such long-lifetime components for mediator-grown WS₂ further corroborates the high performance of the material.

To identify the origin of the enhanced optoelectronic properties of mediator-grown WS₂, we conduct detailed microscopic and electron spectroscopic characterization. Optical microscopy of WS₂ grown after short durations reveals large individual domains of 500 um size (Fig. 4a). Aberration-corrected transmission electron microscopy can resolve the atomic structure of WS₂ and identify individual vacancies[33,34]. Even upon close inspection of large datasets, we observe no evidence of vacancies (Fig. 4b, Supplementary Fig. 3, and Supplementary Note 3). The density of inevitable, transfer-induced damage provides us with an upper limit of defectiveness of $10^{11} cm^{-2}$, which is comparable to

previous lower bounds of defect densities in high-quality WS₂[35]. Selected area electron diffraction (SAED) images show identical orientation across hundreds of micrometers, confirming the large lateral size of single-crystalline domains (Fig. 4c). The absence of edges and lattice defects is reflected in the electronic structure of the grown material. Photoelectron emission spectroscopy demonstrates a position of the Fermi level close to the center of the bandgap (Fig. 4d), indicating the intrinsic nature of WS₂. The extracted Fermi level position of 4.86 eV agrees well with theoretical predictions for vacancy-free WS₂[36]. The measured Fermi level is within 0.5% of the expected intrinsic Fermi level (more details in the Supplementary Note 4) and is 0.2 eV higher than previous reports[36], which corroborates the absence of defect-induced doping.

The characterization results demonstrate the origin of the enhanced optical performance of mediator-grown material is due to the reduction of defects that act as nonradiative recombination centers below the levels of previous synthesis routes.

Application to optoelectronic devices

The high quality and large scale uniformity of the mediator-grown WS₂ permit the realization of electronic devices with unprecedented properties. To illustrate this advance, we focus on photosensors due to their importance for future 2D materials applications and the direct impact of defects on their performance[37]. Different from previous WS₂ growth, mediator-assisted CVD produces continuous films when using sufficiently long growth durations (Fig. 5a), which enables the fabrication of large-scale device arrays (Inset Fig. 5c).
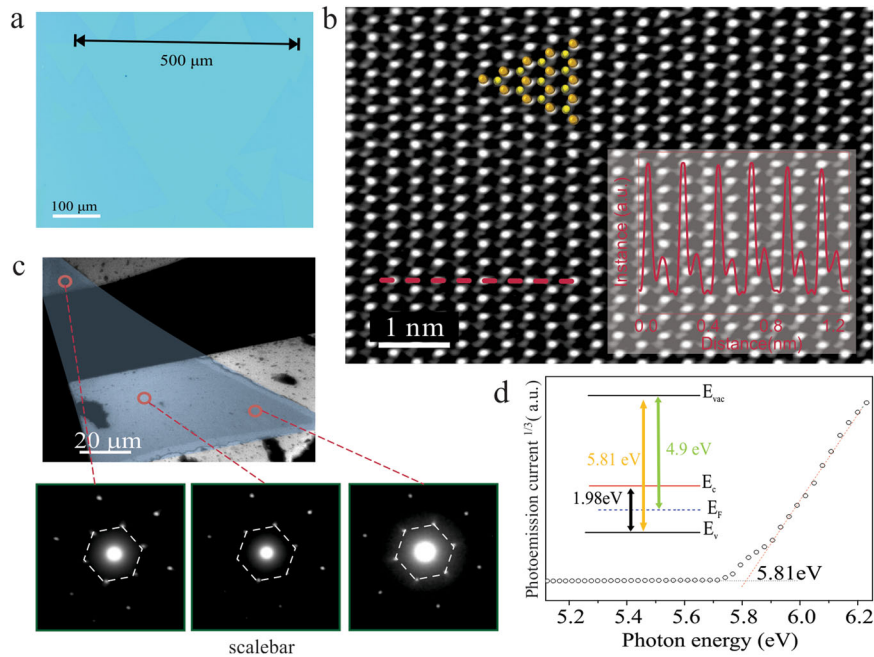
Fig. 4 Detailed characterization of mediator-grown WS₂. a Optical micrograph of individual flake obtained after short growth duration. **b** Aberration corrected TEM image of lattice structure with indication of crystal orientation, (inset) cross-sectional trace of intensity. **c** False-color TEM image of single-crystalline flake, with corresponding SAED patterns at different locations indicating its single crystallinity. **d** Determining valence band edge through linear extrapolation of cubic root of photoelectron emission vs photon energy[48], (inset) experimental band structure with Fermi level extracted from Kelvin-probe measurements.
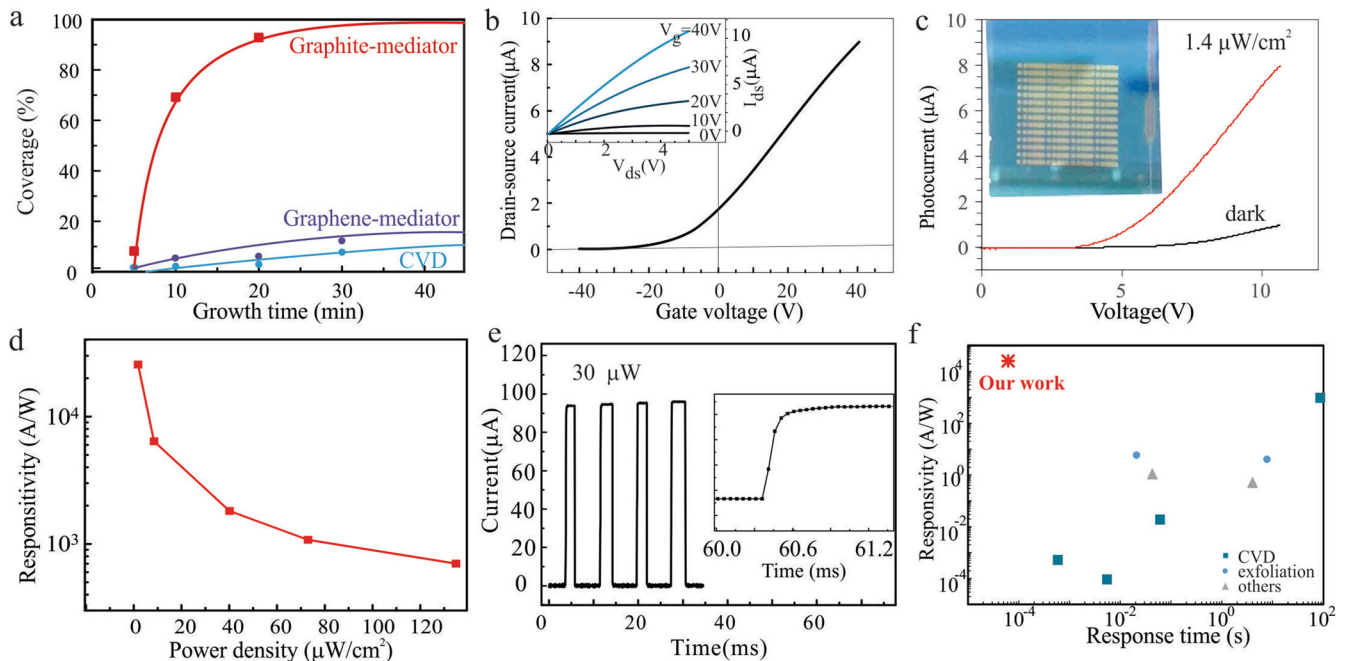

Fig. 5 Application of mediator-grown WS₂. a Comparison of achievable coverage with and without different mediators. **b** Transconductance of FET fabricated from mediator-grown WS₂, (inset) drain-source current-voltage characteristics at different gate voltages. **c** Current-voltage characteristics of graphite mediator-grown WS₂ in dark and illuminated conditions, (inset) photograph of device array. **d** Power-dependent photoresponsivity, **e** current response under pulsed light illumination, (inset) closeup of rising flank. **f** Comparison of device performance to reported values for WS₂ (more details and references in Supplementary Table 1).

FET measurements demonstrate a p-type semiconducting behavior and a mobility of $5\,cm^2Vs^{-1}$ at an intrinsic carrier concentration of $2 \times 10^{11}cm^{-2}$ was extracted (Fig. 5b, more details in Methods). These results agree with previous reports of WS₂ devices on SiO₂ with unoptimized contacts[38].

The photocurrent-voltage characteristics show a clear change in behavior upon illumination (Fig. 5c). Laser-power-dependent measurements show sensitivities of ~25,000 A/W (Fig. 5d), which represents an improvement of several orders of magnitude over previous WS₂ devices[39]. The detectivity D* is estimated to be up to

3.25×10^{14} Jones. This enhanced performance is a direct consequence of the decreased trap density and the low amount of defect-assisted exciton combination.

In the absence of optimized device contacts, the response to pulsed illumination provides information on carrier mobility[40]. We indeed observe a high-speed response with a rise time of 58 µs (Fig. 5e; more information in Supplementary Fig. 7), which to our knowledge represents the fastest 2D material-based sensor device to date. The superior performance of our photosensor device compared to other WS$_2$ photosensors (Fig. 5f) emphasizes the potential of defect-control in enhancing the commercial and scientific prospect of 2D materials.

DISCUSSION

In this study, we have devised an approach to producing defect-free WS$_2$ with superior optoelectronic properties at unprecedented production scale. Mediator-assisted CVD growth was shown to increase the uniformity of WS$_2$ towards the multiwafer scale and enhance its crystalline quality beyond exfoliated 2D materials levels. Such materials exhibit high environmental stability and near-unity quantum yield due to a large decrease in defect concentration. Our approach enables novel optoelectronic devices with record-breaking speed and sensitivity.

METHODS
High throughput WS$_2$ growth

The throughput of mediator-assisted CVD (See Supplementary Fig. 1) can be enhanced by conducting growth in stacks, as illustrated in Fig. S1. Each layer of the stack consists of a growth substrate (Si/300 nm SiO$_2$) and a mediator in direct contact. A 40 nm WO3 film is pre-deposited on top of the mediator (graphite or graphene) by e-beam evaporation. SiOx/Si substrate where WS$_2$ is grown were facing down placed directly on to this WO3/mediator structure. Ten units of graphite/WO3, Si/SiO$_2$ wafers are then stacked.

Growth was conducted in a two-stage heating process: First the temperature is increased from room temperature to 700 degrees in 15 min and then from 700 degrees to 915 degrees in 20 min under an argon flow of 50sccm. After the heating, growth is conducted under a 100 sccm flow of diluted hydrogen sulfide (1% H$_2$S + 99% Ar) for 10 min at 760 mTorr. Finally, the growth temperature is reduced to 830 degrees in 15 min. When the temperature of the furnace tube is lower than 830 degrees, the furnace is open to cool down naturally.

Mediator

Graphite foil (PERMA-FOIL) with a thickness of around 200 µm was used as a mediator. For using graphene as mediator, monolayer Graphene was first grown on copper and then transferred on to SiO$_2$/Si following established procedures[20]. Briefly, polymethyl methacrylate (A9, Microchem) is spin-coated on the copper foil. Secondly, the copper foil is soaked in sodium sulfate for etching, and then washed with deionized water three times. Finally, the single-layer graphene is transferred onto the substrate and placed on a hot plate for drying. After drying, the substrate is soaked in acetone for 1 h to remove PMMA, and acetone was removed with isopropanol. Finally, blow drying with N$_2$ completed the transfer.

Conventional WS$_2$ synthesis

Mediator-grown WS$_2$ was compared to exfoliated and CVD-grown material. WS$_2$ was exfoliated onto SiO$_2$ from bulk crystals using micromechanical cleavage. Conventional CVD growth was conducted following previous reports[41]. Briefly, WS$_2$ was grown on sapphire substrates from MoO3 powder positioned in the heating zone and S powder that was placed 20 cm upstream from the substrate and heated to 300°C. The reaction zone was at a temperature of 875°C protected by an Ar flow of 100sccm under atmospheric pressure. For their optical microscopic images and Raman characterization results, please See Supplementary Fig. 2.

Fermi-level measurement

An APS01 (KP Technology) system was employed to measure the work function of the WS$_2$ using a Kelvin-probe technique and the valence band maximum through photoemission. Both values were combined with the band gap determined by photoemission to yield the band structure.

Thermochemical simulation

We calculate the equilibrium composition for precursors and synthesis products that are connected through a system of reaction equations that considers the reduction of the precursors with and without a carbon mediator and the formation of WS$_2$ from intermediate constituents. This is achieved by minimizing the free energy of each reaction and using mass balance equations as subsidiary conditions[42]. Thermodynamic data for intermediate and final reaction products were obtained from literature[43]. To get the results presented in Fig. 2c, the WS$_2$ reaction yield was calculated for different concentrations of hydrogen sulfide precursor, and a numerical derivative of the yield was calculated. This process was repeated for different concentrations of carbon mediator.

Grain size and growth rate measurements

Several optical micrographs were taken for each sample location and the size of at least 20 grains was measured for each sample position using Gwyddion image processing. The growth rate was calculated by conducting grain-size measurements after varying growth durations and fitting their extent to a linear size-time relationship.

Photoluminescence and Quantum Yield Measurement

A customized microscopic Photoluminescence spectroscopy system equipped with a 532 nm laser is utilized for WS$_2$ PL and quantum yield measurements. The spot size is estimated to be ~10 µm^2. The WS$_2$ PL mapping measurement integrates PL intensity in the peak position range from 610 nm to 640 nm.

The WS$_2$ PL quantum yield is defined by comparing its emission intensity to Rhodamine 6 G (R6G), which possesses near 100% quantum yield efficiency[44] using a procedure, which has previously been used to measure the QY of 2D materials[45,46]. Briefly, a diluted solution of R6G (300 uM in methanol) was spin-coated onto a glass slide to confirm its emission efficiency in comparison to its absorption (obtained by millimeter-scale transmittance measurements). With the emission efficiency calibrated, the same approach was applied to WS$_2$ to extract its quantum efficiency.

Transistor fabrication

Backgated FETs were produced from mediator-grown WS$_2$ on silicon wafers with 300 nm oxide. First, channels were defined by lithographical patterning and CF4 plasma etching. Then, in a second step, electrical contacts were patterned lithographically to form channels with a width of 10 um and a length of 8 um. Electrodes were produced from 30 nm gold by thermal evaporation. The silicon wafer was utilized as the gate and current-voltage characteristics were measured with a Keysight B2912A source meter.

The mobility was extracted from the slope of the transconductance according to:

$$\mu = \frac{L}{W} \frac{1}{C_g V_{ds}} \frac{dI_{ds}}{dV_g}, \tag{1}$$

where C_g is the gate capacitance of the silicon oxide layer and L/W is the ratio of channel length and width.

With this mobility, the carrier density n_{2D} can be estimated in the linear region of the drain-source current according to[47]

$$I_{DS} = q n_{2D} W \mu \frac{V_{ds}}{L}. \tag{2}$$

Photodetector measurement

A custom-made system with a Xenon white light source that was connected to a CM-110 monochromator and output with an optical fiber. For measuring photocurrent, the fiber was connected to an optical microscope and the power measure under the objective were 100 nW cm^{-2}. A Keysight B2912A source meter was employed to measure the

photocurrent. The power dependent photocurrent was extracted at 15 V and the maximum value of 25,000 AW^{-1} were obtained under power of 1.4 $\mu W\ cm^{-2}$. The photoresponse time was measured under a power of 30 $\mu W\ cm^{-2}$ using a SR-540 optical chopper (also See Supplementary Note 7). Each device had dimensions of 400 μm(W) x 50 μm(L).

DATA AVAILABILITY

The data of this study are available from the corresponding author upon reasonable request.

REFERENCES

1. Glavin, N. R. et al. Emerging Applications of Elemental 2D Materials. *Adv. Mater.* **32**, 1904302 (2020).
2. Li, H., Huang, J.-K., Shi, Y. & Li, L.-J. Toward the Growth of High Mobility 2D Transition Metal Dichalcogenide Semiconductors. *Adv. Mater. Interfaces* **6**, 1900220 (2019).
3. Liang, Q., Zhang, Q., Zhao, X., Liu, M. & Wee, A. T. S. Defect Engineering of Two-Dimensional Transition-Metal Dichalcogenides: Applications, Challenges, and Opportunities. *ACS Nano* **15**, 2165–2181 (2021).
4. Schaibley, J. R. et al. Valleytronics in 2D materials. *Nat. Rev. Mater.* **1**, 16055 (2016).
5. Zhang, W., Huang, Z., Zhang, W. & Li, Y. Two-dimensional semiconductors with possible high room temperature mobility. *Nano Res.* **7**, 1731–1737 (2014).
6. Aji, A. S., Solís-Fernández, P., Ji, H. G., Fukuda, K. & Ago, H. High Mobility WS_2 Transistors Realized by Multilayer Graphene Electrodes and Application to High Responsivity Flexible Photodetectors. *Adv. Func. Mater.* **27**, 1703448 (2017).
7. Cong, C., Shang, J., Wang, Y. & Yu, T. Optical Properties of 2D Semiconductor WS_2. *Adv. Opt. Mater.* **6**, 1700767 (2018).
8. Fabbri, F. et al. Edge Defects Promoted Oxidation of Monolayer WS_2 Synthesized on Epitaxial Graphene. *J. Phys. Chem. C.* **124**, 9035–9044 (2020).
9. Enyashin, A. N., Bar-Sadan, M., Houben, L. & Seifert, G. Line Defects in Molybdenum Disulfide Layers. *J. Phys. Chem. C.* **117**, 10842–10848 (2013).
10. Vancso, P. et al. The intrinsic defect structure of exfoliated MoS2 single layers revealed by Scanning Tunneling Microscopy. *Sci. Rep.* **6**, 29726 (2016).
11. Kim, I. S. et al. Influence of Stoichiometry on the Optical and Electrical Properties of Chemical Vapor Deposition Derived MoS2. *ACS Nano* **8**, 10551–10558 (2014).
12. Wang, S. et al. Shape Evolution of Monolayer MoS2 Crystals Grown by Chemical Vapor Deposition. *Chem. Mater.* **26**, 6371–6379 (2014).
13. Zhou, J. et al. A library of atomically thin metal chalcogenides. *Nature* **556**, 355–359 (2018).
14. Momeni, K., Ji, Y., Zhang, K., Robinson, J. A. & Chen, L.-Q. Multiscale framework for simulation-guided growth of 2D materials. *npj 2D Mater. Appl.* **2**, 27 (2018).
15. Pedersen, H. Time as the Fourth Dimension: Opening up New Possibilities in Chemical Vapor Deposition. *Chem. Mater.* **28**, 691–699 (2016).
16. Kobayashi, Y. et al. Growth and Optical Properties of High-Quality Monolayer WS_2 on Graphite. *ACS Nano* **9**, 4056–4063 (2015).
17. Chubarov, M. et al. Wafer-Scale Epitaxial Growth of Unidirectional WS_2 Monolayers on Sapphire. *ACS Nano* **15**, 2532–2541 (2021).
18. Zhang, Z. W. et al. Ultrafast growth of large single crystals of monolayer WS_2 and WSe2. *Natl Sci. Rev.* **7**, 737–744 (2020).
19. Fu, Q. et al. Controllable synthesis of high quality monolayer WS_2 on a SiO2/Si substrate by chemical vapor deposition. *RSC Adv.* **5**, 15795–15799 (2015).
20. Hsieh, Y.-P., Shih, C.-H., Chiu, Y.-J. & Hofmann, M. High-Throughput Graphene Synthesis in Gapless Stacks. *Chem. Mater.* **28**, 40–43 (2016).
21. Yang, P. et al. Influence of seeding promoters on the properties of CVD grown monolayer molybdenum disulfide. *Nano Res.* **12**, 823–827 (2019).
22. Lan, C. et al. Wafer-scale synthesis of monolayer WS_2 for high-performance flexible photodetectors by enhanced chemical vapor deposition. *Nano Res.* **11**, 3371–3384 (2018).
23. Chin, H. T. et al. How does graphene grow on complex 3D morphologies? *Phys. Chem. Chem. Phys.* **19**, 23357–23361 (2017).
24. Koçak, Y. & Gür, E. Growth Control of WS_2: From 2D Layer by Layer to 3D Vertical Standing Nanowalls. *ACS Appl. Mater. Interfaces* **12**, 15785–15792 (2020).
25. Zheng, B. et al. WO(3)-WS(2) Vertical Bilayer Heterostructures with High Photoluminescence Quantum Yield. *J. Am. Chem. Soc.* **141**, 11754–11758 (2019).
26. Jin, H. et al. Effects of Direct Solvent-Quantum Dot Interaction on the Optical Properties of Colloidal Monolayer WS_2 Quantum Dots. *Nano Lett.* **17**, 7471–7477 (2017).
27. Goodman, A. J., Willard, A. P. & Tisdale, W. A. Exciton trapping is responsible for the long apparent lifetime in acid-treated MoS2. *Phys. Rev. B* **96**, 121404 (2017).
28. Hu, Z. et al. Two-dimensional transition metal dichalcogenides: interface and defect engineering. *Chem. Soc. Rev.* **47**, 3100–3128 (2018).
29. Paradisanos, I. et al. Room temperature observation of biexcitons in exfoliated WS_2 monolayers. *Appl. Phys. Lett.* **110**, 193102 (2017).
30. Cui, Q. L. et al. Robust and High Photoluminescence in WS_2 Monolayer through In Situ Defect Engineering. *Adv. Funct. Mater.* **31**, 2105339 (2021).
31. Lin, Y.-C. et al. Revealing the Atomic Defects of WS_2 Governing Its Distinct Optical Emissions. *Adv. Funct. Mater.* **28**, 1704210 (2018).
32. Palummo, M., Bernardi, M. & Grossman, J. C. Exciton Radiative Lifetimes in Two-Dimensional Transition Metal Dichalcogenides. *Nano Lett.* **15**, 2794–2800 (2015).
33. Aryeetey, F., Ignatova, T. & Aravamudhan, S. Quantification of defects engineered in single layer MoS2. *Rsc Adv.* **10**, 22996–23001 (2020).
34. Zhang, J. Y. et al. Characterization of atomic defects on the photoluminescence in two-dimensional materials using transmission electron microscope. *InfoMat* **1**, 85–97 (2019).
35. Rosenberger, M. R., Chuang, H. J., McCreary, K. M., Li, C. H. & Jonker, B. T. Electrical Characterization of Discrete Defects and Impact of Defect Density on Photoluminescence in Monolayer WS_2. *ACS Nano* **12**, 1793–1800 (2018).
36. Wang, X. et al. Defect Heterogeneity in Monolayer WS_2 Unveiled by Work Function Variance. *Chem. Mater.* **31**, 7970–7978 (2019).
37. Wang, J., Han, J., Chen, X. & Wang, X. Design strategies for two-dimensional material photodetectors to enhance device performance. *InfoMat* **1**, 33–53 (2019).
38. Ovchinnikov, D., Allain, A., Huang, Y. S., Dumcenco, D. & Kis, A. Electrical Transport Properties of Single-Layer WS_2. *ACS Nano* **8**, 8174–8181 (2014).
39. Perea-López, N. et al. Photosensor Device Based on Few-Layered WS_2 Films. *Adv. Funct. Mater.* **23**, 5511–5517 (2013).
40. Tiwari, S. & Greenham, N. C. Charge mobility measurement techniques in organic semiconductors. *Opt. Quantum Electron.* **41**, 69–89 (2009).
41. Liu, P. Y. et al. Large-Area WS_2 Film with Big Single Domains Grown by Chemical Vapor Deposition. *Nanoscale Res. Lett.* **12**, 1–10 (2017).
42. Carlsson, J. O. Thermochemical modeling of interfacial reactions and selective deposition at growth from the vapor. *J. Vac. Sci. Technol. A* **6**, 1656–1662 (1988).
43. Rössler, U. & Schulz, M. SpringerMaterials-The Landolt-Börnstein Database (http://www.springermaterials.com).
44. Magde, D., Wong, R. & Seybold, P. G. Fluorescence quantum yields and their relation to lifetimes of rhodamine 6G and fluorescein in nine solvents: Improved absolute standards for quantum yields. *Photochem. Photobiol.* **75**, 327–334 (2002).
45. Amani, M. et al. Near-unity photoluminescence quantum yield in MoS2. *Science* **350**, 1065–1068 (2015).
46. Wang, H., Zhang, C. & Rana, F. Ultrafast dynamics of defect-assisted electron–hole recombination in monolayer MoS2. *Nano Lett.* **15**, 339–345 (2015).
47. Huo, N. J. et al. Photoresponsive and Gas Sensing Field-Effect Transistors based on Multilayer WS_2 Nanoflakes. *Sci. Rep.* **4**, 1–9 (2014).
48. Shlyakhov, I. et al. Internal photoemission of electrons from 2D semiconductor/3D metal barrier structures. *J. Phys. D: Appl. Phys.* **54**, 295101 (2021).

AUTHOR CONTRIBUTIONS

Y.C. conducted large-scale growth experiments, S.C. carried out the growth analysis, D.L. conducted the comparison of different mediator. C.L. optimized the growth parameter, H.T. optimized the surface treatment of substrate. Y.Y. increased the growth scale. H.S. assisted with lifetime measurement. G.H. provides the exfoliated WS_2. M.K. revised the manuscript. C.T. characterized the PL of WS_2, Y.F. suggests the mediator model, M.H. supervised the simulation, Y.H. led the project and wrote the draft.

COMPETING INTERESTS

The authors declare no competing interests.

ADDITIONAL INFORMATION

Supplementary information The online version contains supplementary material available at https://doi.org/10.1038/s41699-022-00329-1.

Correspondence and requests for materials should be addressed to Ya-Ping Hsieh.

Reprints and permission information is available at http://www.nature.com/reprints

Publisher's note Springer Nature remains neutral with regard to jurisdictional claims in published maps and institutional affiliations.